Microporous and Mesoporous Materials 181 (2013) 141–145

Contents lists available at SciVerse ScienceDirect

Microporous and Mesoporous Materials

journal homepage: www.elsevier.com/locate/micromeso

Easy hydrothermal synthesis of external mesoporous γ-Al_2O_3 nanorods as excellent supports for Au nanoparticles in CO oxidation

Jie Wang, Ke Shang, Yue Guo, Wen-Cui Li *

State Key Laboratory of Fine Chemicals, School of Chemical Engineering, Dalian University of Technology, Dalian 116024, PR China

ARTICLE INFO

Article history:
Received 12 May 2013
Received in revised form 28 June 2013
Accepted 19 July 2013
Available online 29 July 2013

Keywords:
Nanorods
Alumina
External mesopores
Gold catalyst
CO oxidation

ABSTRACT

External mesoporous γ-Al_2O_3 nanorods with an aspect ratio of 2–4 has been hydrothermally synthesized using $Al(NO_3)_3{\cdot}9H_2O$ as precursor and $(NH_4)_2CO_3$ as precipitant without any templates and followed by a calcination step. The obtained samples were characterized by thermogravimetric analysis (TG), X-ray powder diffraction (XRD), nitrogen sorption, Fourier transform infrared spectrometry (FT-IR), and scanning transmission electron microscopy (STEM). It can be confirmed that the morphology of nanorods is formed in the low-temperature hydrothermal process of 100 °C. Through the thermal decomposition of intermediate product $NH_4Al(OH)_2CO_3$, the prepared γ-Al_2O_3 possesses abundant external mesopores, which can act as "holders" to stabilize or anchor gold nanoparticles efficiently. Using CO oxidation as an probe reaction, the results demonstrated that Au catalyst exhibited excellent catalytic performance with the complete CO conversion at 18 °C ($T_{50\%}$ = −11.2 °C) and reactive stability over 166 h under a space rate of 134,000 mL h^{-1} $g_{cat}{}^{-1}$.

1. Introduction

In recent years, considerable efforts have been devoted to synthesize nanomaterials with controllable morphologies and nanostructures to achieve desired properties. Due to the remarkable advantages of γ-Al_2O_3 such as high surface area, good mechanical and especially thermal and chemical stability etc., the synthesis of alumina with controllable nanostructures is still a very hot topic for both academic study and practical application. Besides, alumina has diverse functions and can be widely used as catalysts [1], catalyst supports [2,3], and absorbents [4,5].

It has been known that alumina with different morphology and nanostructure has a significant influence on the performance of catalysts. Taking Au/Al_2O_3 catalyst as examples, mesoporous γ-Al_2O_3 can hold a high dispersion of gold nanoparticles and such Au/Al_2O_3 catalyst showed an excellent activity for liquid-phase alcohol oxidations [2,6]. In addition, hydrothermally synthesized flake-like alumina using urea as precipitant enables to stabilize gold nanoparticles with small sizes and high dispersion, even after annealing of the catalyst to 700 °C [7]. When using γ-Al_2O_3 nanofibers as the support, the activity of Au catalyst for CO oxidation could be remarkably improved, as compared to using commercial γ-Al_2O_3 support [8]. Thus, the current scientific interest is to develop a simple and effective strategy to produce goal-oriented porous aluminum oxides with the abovementioned architecture and properties for various applications.

To date, a series of γ-Al_2O_3 with special morphologies and nanostructures can be achieved through a hydrothermal or solvothermal route by varying the types of ionic or nonionic surfactants, Al^{3+} precursors and solvents [9–13]. Specifically, it has been reported that fibrous crystallites of γ-Al_2O_3 about 3–4 nm thick and 30–60 nm long can be obtained, using $NaAlO_2$ and nonionic poly (ethylene oxide) surfactants [14]. Bearing the fact in mind that Au loaded on the fiber-structured alumina always show a much high catalytic activity [8], we thus quickly scaned the related literatures considering the hydrothermal synthesis of alumina nanorods or nanofibers [8,15–21] (summarized in Table S1), and found that there is still a great challenge to obtain uniform alumina material with specific morphology under a moderate reaction conditions in the aim of achieving a high active Au/Al_2O_3 catalyst.

In our previous work, the flake-like alumina was prepared through a hydrothermal route using $Al(NO_3)_3{\cdot}9H_2O$ as precursor and urea as precipitant and followed by a calcination step [7], which showed a good thermostability and catalytic activity in CO oxidation after gold loading. As is known that urea hydrolysis proceeds in two steps: formation of ammonium cyanate (NH_4CNO) and subsequent hydrolysis of NH_4CNO to ammonium carbonate ($(NH_4)_2CO_3$) [22]. Therefore, we conceive a direct use of $(NH_4)_2CO_3$ instead of urea as precipitant to prepare alumina with certain morphology. $Al(NO_3)_3{\cdot}9H_2O$ can produce complexes with $(NH_4)_2CO_3$ in the form of ammonium aluminum carbonate hydroxide ($NH_4Al(OH)_2CO_3$) at the low temperature [23]. It is expected that the

* Corresponding author. Fax: +86 411 84986355.
E-mail address: wencuili@dlut.edu.cn (W.-C. Li).

1387-1811/$ - see front matter © 2013 Elsevier Inc. All rights reserved.
http://dx.doi.org/10.1016/j.micromeso.2013.07.028

release of NH_3, CO_2 and H_2O during the thermal decomposition process of $NH_4Al(OH)_2CO_3$ could create some pores or defects on the final product of alumina external surface, which will potentially play a major role in the stabilization of noble metal nanoparticles, for example, gold nanoparticles, to avoid an obvious sintering. As a result, an easy hydrothermal synthesis of γ-Al_2O_3 nanorods with numerous external mesopores is developed by using inorganic aluminum salt $Al(NO_3)_3{\cdot}9H_2O$ as precursor and $(NH_4)_2CO_3$ as precipitant without any templates. As this structure of γ-Al_2O_3 support would ideally stabilize Au nanoparticles, the obtained Au catalysts exhibits enhanced catalytic performance towards CO oxidation. This study could be distinguished by its low-cost and easy synthesis method, special external mesopores structure of γ-Al_2O_3 and excellent activity of supported gold catalyst for CO removal.

2. Experimental

2.1. Synthesis of γ-Al_2O_3 nanorods

Typically, $Al(NO_3)_3{\cdot}9H_2O$ and $(NH_4)_2CO_3$ with a molar ratio of 1:9 was dissolved in deionized water, and the concentration of Al^{3+} was 0.02 M. The obtained mixture was transferred into a 150 mL Teflon-lined stainless steel autoclave and heated at 100 °C for 24 or 36 h. Then the white precipitates were washed with deionized water and dried at 90 °C. After a calcination step at 800 °C for 2 h, the final products were obtained and named as Al_2O_3-1 and Al_2O_3-2, respectively.

2.2. Preparation of Au/Al_2O_3 catalyst and catalytic test

Au nanoparticles were deposited on the γ-Al_2O_3 nanorods by a deposition–precipitation method with $HAuCl_4$ solution (7.9 g L^{-1}) at pH 8–9 in 60 °C for 2 h. After washing and drying, the precipitants were thermal treated at 250 °C for 2 h in air to generate the Au/Al_2O_3 catalysts, denoted as Au-(Al_2O_3-1) and Au-(Al_2O_3-2), respectively. The Au content was theoretically estimated as 3 wt.%. The activity of Au catalysts for CO oxidation was evaluated in a fixed bed quartz reactor using 50 mg of catalyst (20–40 mesh) with a composition of 1 vol.% CO, 20 vol.% O_2 and 79 vol.% N_2 and the total rate of feed gas was 67 mL min^{-1} (80,000 mL h^{-1} g_{cat}^{-1}). The products were analyzed using a GC-7890 gas chromatograph equipped with a thermal conductivity detector.

2.3. Characterization

Thermogravimetric and differential scanning calorimetry analysis (TG-DSC) were conducted on a thermogravimetric analyzer STA 449 F3 (NETZSCH), under air atmosphere with a heating rate of 10 °C min^{-1}. X-ray diffraction patterns (XRD) were obtained with a D/MAX-2400 diffractometer using Cu Kα radiation (40 kV, 100 mA, λ = 1.54056 Å). Nitrogen adsorption/desorption isotherms were measured with a TriStar 3000 adsorption analyzer (Micromeritics) at liquid nitrogen temperature. The samples were degassed at 200 °C for 4 h prior to analysis. The Brunauer–Emmett–Teller (BET) method was utilized to calculate the specific surface areas (S_{BET}). Pore size distributions (PSDs) were derived from the desorption branches of the isotherms using the Barrett–Joyner–Halenda (BJH) model. Infrared Fourier transform spectra (FT-IR) were recorded using a Nicolet 6700 FT-IR spectrometer at a resolution of 4 cm^{-1} and scale at 4000–640 cm^{-1}. Transmission electron microscope (TEM) images were obtained with a Tecnai $G^2$20 S-Twin microscope with accelerative voltage of 200 kV. HAADF-STEM images were obtained on a JEOL2010F instrument by using an electron probe (0.5 nm diameter) at a diffraction camera length of 10 cm. Scanning electron microscope (SEM) images were obtained from a Hitachi S-4800 instrument. The actual gold content was analyzed using an inductively coupled plasma atomic emission spectrometer (ICP-AES) on the Optima 2000 DV.

3. Results and discussion

3.1. Synthesis of γ-Al_2O_3 nanorods

To begin with, one sample (named as Al_2O_3-1-hydro) was collected after hydrothermal treatment for 24 h and analyzed by TG-DSC measurement under air to explore the thermal decomposition behavior. As seen in Fig. 1a, the weight loss (~63.0%) below 300 °C is mainly attributed to the release of adsorbed water and the decomposition of Al_2O_3-1-hydro sample. Thus, we deduce that $NH_4Al(OH)_2CO_3$ is the primary component of Al_2O_3-1-hydro ($2NH_4Al(OH)_2CO_3 \rightarrow Al_2O_3 + 2CO_2 + 2NH_3 + 3H_2O$, theory weight loss value is 63.3%) [16]. The DSC curve displays a broad exothermic peak at ~400 °C, which represents the decomposition of $NH_4Al(OH)_2CO_3$ and the phase transformation to γ-Al_2O_3. As the temperature increases to 800 °C, almost no obvious weight loss can be observed, Al_2O_3-1-hydro sample was therefore calcined at 800 °C to obtain sample Al_2O_3-1. The samples Al_2O_3-1-hydro and Al_2O_3-1 then were characterized with FT-IR.

The FT-IR spectra of Al_2O_3-1-hydro in Fig. 1b shows that the peaks at 1452 and 1539 cm^{-1} are ascribed to stretching modes of CO_3^{2-} [24]. And the characteristic bands of NH_4^+ (ν_{NH} at 3170, 3005, and 2840 cm^{-1}; δ_{NH} at 1830 and 1720 cm^{-1}) can also be observed [25]. This is consistent with the results of TG-DSC that $NH_4Al(OH)_2CO_3$ is recognized as the final hydrothermal product, when using $(NH_4)_2CO_3$ as precipitant. The intensive peaks at 1160 and 1070 cm^{-1} are due to the δ_{as} Al–O–H and δ_s Al–O–H modes, and the bands observed at 746 cm^{-1} represent the stretching modes of AlO_6. In the case of Al_2O_3-1 sample after annealing at 800 °C for 2 h, the band at 3408 cm^{-1} and weak band at 1638 cm^{-1} are attributed to the stretching vibrations of OH group that is mainly caused by physically adsorbed water in alumina surface [26]. The absorption peaks of carbonate and ammonium almost disappear, indicating a complete decomposition of $NH_4Al(OH)_2CO_3$ and formation of alumina.

Fig. 1c exhibits the XRD patterns of samples Al_2O_3-1 and Al_2O_3-2. There into, Al_2O_3-2 was prepared by prolonging hydrothermal time to 36 h and the rest treatment conditions are the same as sample Al_2O_3-1. The characteristic peaks of both the calcined samples can unambiguously be attributed to γ-Al_2O_3 phase (JCPDS No. 10-0425). In particular, the crystallinity of alumina products is improved as the increase of hydrothermal time. The pore structures of the obtained γ-Al_2O_3 were further characterized by nitrogen sorption measurement at −196 °C. As shown in Fig. 1d, the N_2 sorption isotherms of Al_2O_3-1 and Al_2O_3-2 are essentially of type IV, and the capillary condensation step at P/P_0 = 0.45–1.0 indicates the existence of abundant mesopores. The corresponding pore size distributions (PSDs) suggest a mesopore size centered at 4 nm. Detailed textural parameters and synthesis conditions of γ-Al_2O_3 are listed in Table 1. The surface areas of both samples are around 150–160 m^2 g^{-1}, which is mainly due to a relative high calcination temperature of 800 °C. In addition, the sample Al_2O_3-1-hydro without further calcination was also characterized by nitrogen sorption measurement. As shown in Fig. S1, the isotherm of Al_2O_3-1-hydro has a sharp capillary condensation step at P/P_0 = 0.8–1.0, indicating the presence of larger pores from the closely packed Al_2O_3-1-hydro nanorods. The surface area is only 46 m^2 g^{-1} and almost no ~4 nm mesopores were detected in the Al_2O_3-1-hydro, implying the abundant mesopores were produced in the process of calcination.

Furthermore, the morphologies of the samples were characterized by STEM and TEM techniques. It can be clearly seen in Fig. 2a and c that γ-Al_2O_3 samples display uniform nanorods structure

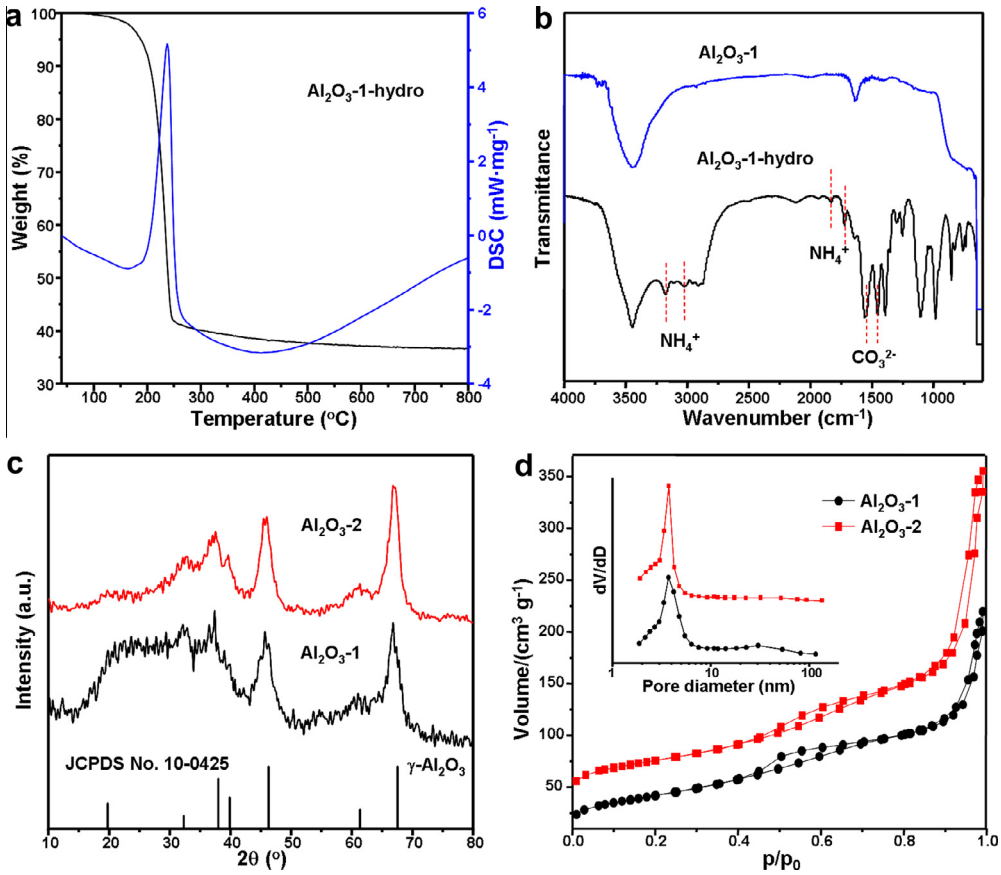

Fig. 1. TG and DSC curves (a) of Al_2O_3-1-hydro, FT-IR curves (b) of Al_2O_3-1-hydro and Al_2O_3-1. XRD patterns (c) and N_2 isotherms of alumina supports ((d), inset are the corresponding pore size distribution). The isotherms of Al_2O_3-2 were offset up by 30 $cm^3\ g^{-1}$.

Table 1
Textural parameters of γ-Al_2O_3 materials and the catalytic activity of Au catalysts.

Support	S_{BET} ($m^2\ g^{-1}$)[a]	V_{total} ($cm^3\ g^{-1}$)[a]	D_{peak} (nm)[a]	Au content (wt.%)[b]	$T_{50\%}$ (°C)[c]	$T_{100\%}$ (°C)[c]	X_{CO} (%)[d]	Rate (mol $h^{-1}\ g_{Au}^{-1}$)[d]
Al_2O_3-1	165	0.504	4	2.4	7.0	40.0	31.0	0.456
Al_2O_3-2	152	0.340	4	2.7	−11.2	18.0	89.0	1.201

[a] S_{BET} = specific surface area calculated by the Brunauer–Emmett–Teller (BET) method, V_{total} = total pore volumes at P/P_0 = 0.997, D_{peak} = pore sizes at maxima of the pore size distributions (PSDs).
[b] Au content was detected by ICP technique.
[c] $T_{50\%}$ and $T_{100\%}$ represent the temperatures for 50% and 100% CO conversion, respectively.
[d] X_{CO} stands for the CO conversion at 0 °C and the corresponding reactive rate of Au catalyst at 0 °C.

with length in 90–140 nm and diameter in 35–45 nm (aspect ratio around 2–4). Particularly, as shown in Fig. 2b and d, the surfaces of nanorods are quite rough and possess numerous small mesopores with the average sizes of 3.0 ± 0.5 nm, which are consistent with the results deduced from nitrogen sorption measurement as well. The above results demonstrate our strategy of creating external mesopores on γ-Al_2O_3 nanorods can be realized by the calcination of hydrothermal products Al_2O_3-1-hydro and Al_2O_3-2-hydro. If $Al(NO_3)_3{\cdot}9H_2O$ was only subject to a room temperature precipitation with $(NH_4)_2CO_3$ for 30 min without further hydrothermally treatment, the direct calcination of the obtained precipitates consequently led to formation of irregular-shaped γ-Al_2O_3 (Fig. S2a), suggesting that the hydrothermal procedure can crystallize the amorphous gel from the direct precipitation process.

Considering the strategy of producing external mesopores on γ-Al_2O_3 surface, it is wise to utilize excessive amount of precipitant $(NH_4)_2CO_3$ in order to release NH_3, CO_2 and H_2O during the thermal decomposition of intermediate product $NH_4Al(OH)_2CO_3$ with the elevating temperature. Thus, the molar ratio of Al^{3+} and $(NH_4)_2CO_3$ was chosen as 1:9 in this case, which is much higher than the theory ratio of 1:2. Initially, the nuclei were obtained during the reaction of $Al(NO_3)_3$ and $(NH_4)_2CO_3$ in the aqueous solution, as the following proposed reaction:

$$Al(NO_3)_3 + 2(NH_4)_2CO_3 + H_2O \rightarrow 3NH_4NO_3 + NH_4Al(OH)_2CO_3 + CO_2$$

When the suspension was hydrothermally treated at 100 °C for 24 h, the nuclei grew to form $NH_4Al(OH)_2CO_3$ nanorods through the oriented attachment mechanism [13,21,27]. During the thermal decomposition of $NH_4Al(OH)_2CO_3$, γ-Al_2O_3 nanorods with numerous mesopores on the external surface can be achieved after calcination by releasing NH_3, CO_2 and H_2O. In literatures, it was believed that the surfactant micelles played a significant role in directing the assembly of aluminum hydrate particles through hydrogen bonding to form nanorod or nanofiber morphology [15,16]. In our case, γ-Al_2O_3 nanorods can be uniformly fabricated through the hydrothermal treatment at 100 °C for 24 h in the

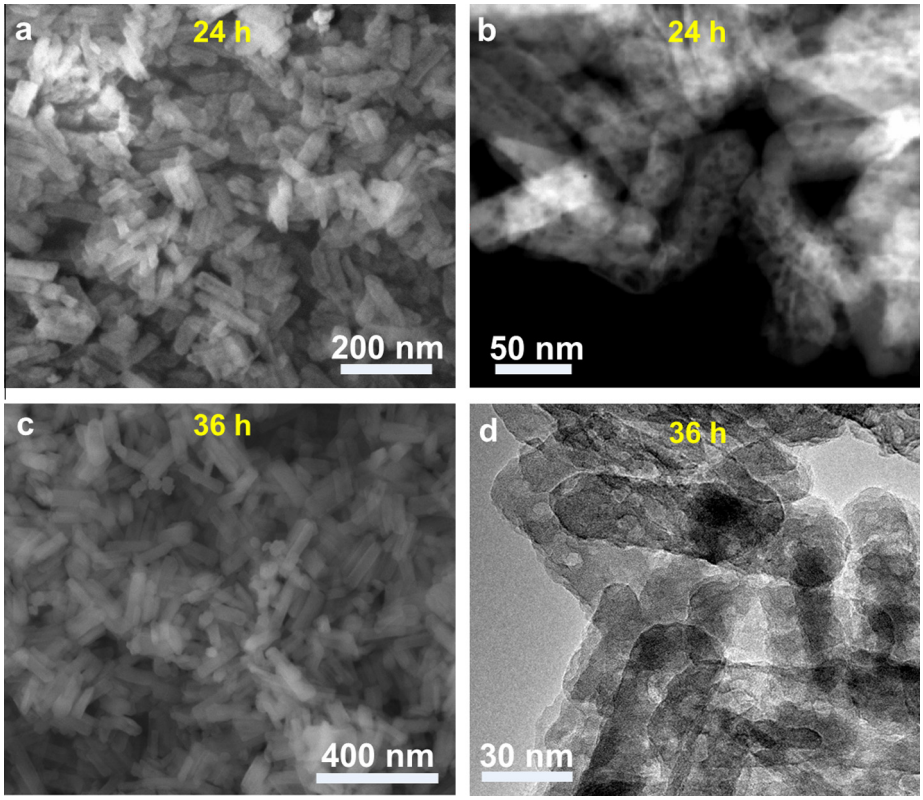

Fig. 2. SEM and STEM images of Al_2O_3-1 (a and b), SEM and TEM images of Al_2O_3-2 (c and d).

absence of surfactant, organic solvent, or hard templates. If we collected the intermediate sample hydrothermally treated 16 h being subject to a SEM characterization, we observed that the alumina nanorods were gradually formed by self-assembly of oriented shorter nanorods in the supersaturated steam environment, as shown in Fig. S2b, which further confirmed that the growth mechanism of nanorods could follow the oriented attachment mechanism.

3.2. Au/Al_2O_3 catalyst for CO oxidation

In general, among the non-reducible oxides, Au catalysts supported on γ-Al_2O_3 are intrinsically less active [28]. However, it was proposed that the reducibility and oxygen activation ability of the support does not seem to be the decisive factor of Au catalyst. This indicates that highly active supported catalysts can be prepared by utilizing the conventional "inert" γ-Al_2O_3 as catalytic support [8,16,29]. Herein, gold nanoparticles as active species were deposited on the obtained mesoporous γ-Al_2O_3 nanorods by deposition–precipitation (DP) method. As a simple and typical probe reaction, CO oxidation was selected to identify the promotion of abundant external mesopores for the catalytic performance of Au catalysts.

As clearly seen in Fig. 3a and Table 1, gold nanoparticles deposited on Al_2O_3-1 and Al_2O_3-2 nanorods are able to achieve a complete conversion of CO at 40 and 18 °C, respectively. Compared with the catalytic activity of Au-(Al_2O_3-1), a better activity of Au-(Al_2O_3-2) should be attributed to the higher crystallinity and a little higher gold content of 2.7 wt.%. In addition, as shown in Table 1, the reactive rate at 0 °C for Au-(Al_2O_3-2) was calculated as 1.201 mol h^{-1} g_{Au}^{-1}, which is comparable and even higher to the results in literatures [2,7,30–33].

Furthermore, a long-term stability test of Au-(Al_2O_3-1) sample was conducted under reaction atmosphere at 30 °C with an increased space rate of 134,000 mL h^{-1} g_{cat}^{-1} (Fig. 3b). Remarkably, no decline of catalytic activity was observed within 102 h (initial 60% CO conversion). Then alternated in turning off and turning on the reaction gas for each 12 h, the CO conversion of Au catalyst has slightly increased to 65% for another three days. After stability test, the used Au-(Al_2O_3-1) sample was observed by TEM images (Fig. 3c and d), gold nanoparticles with average sizes of 2.5 ± 1.0 nm are highly dispersed or anchored on the rough surface of Al_2O_3-1 nanorods, which may contribute to the extraordinary activity and long−term stability of the Au catalyst. The outstanding stability could be relating to the unique nanostructure of such γ-Al_2O_3 nanorods with accessible external mesopores, which can act as "holders" to stabilize gold nanoparticles. In addition, the activity of Au/Al_2O_3 catalyst calcined at 700 °C in Fig. S3 indicates the high thermal stability of the catalyst we made as well. In our previous work, a conventional Al_2O_3 with an undefined morphology was prepared through a precipitation method using $Al(NO_3)_3 \cdot 9H_2O$ and $(NH_4)_2CO_3$ as precursors. Then after loading gold nanoparticles, the Au/conventional Al_2O_3 catalyst calcined at 250 °C can achieve a complete CO conversion at 100 °C and shows no activity after calcined at 700 °C [7]. It suggests that Al_2O_3 nanorods with external mesopores exhibit excellent catalytic behaviors after loading Au nanoparticles.

4. Conclusions

In summary, this work demonstrated that γ-Al_2O_3 nanorods with an aspect ratio of 2–4 were hydrothermally prepared at a low temperature of 100 °C by utilizing $Al(NO_3) \cdot 9H_2O$ as precursor and $(NH_4)_2CO_3$ as precipitant without any temples. In particular, the use of excess $(NH_4)_2CO_3$ leads to the abundant external mesopores formed on the γ-Al_2O_3 surface through the thermal decomposition process of intermediate product $NH_4Al(OH)_2CO_3$. These

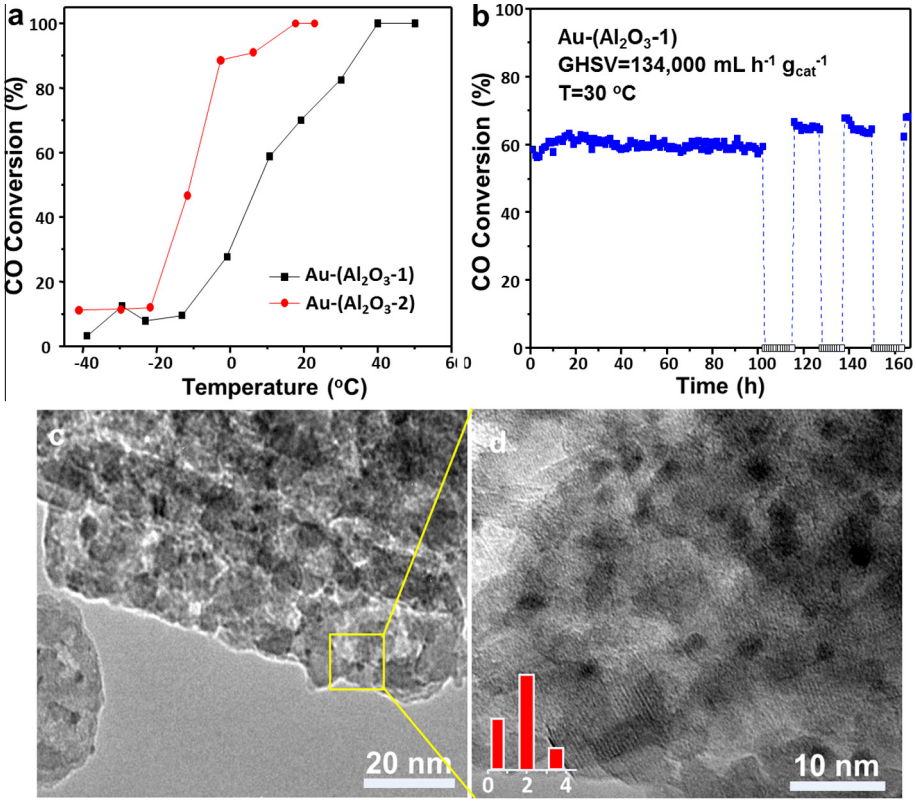

Fig. 3. CO conversion curves of Au catalysts (a), the stability curve of Au-(Al_2O_3-1) in reaction atmosphere at 30 °C with space rate of 134,000 mL h^{-1} g_{cat}^{-1} (b) and the corresponding TEM images of Au-(Al_2O_3-1) after stability test (c and d).

external mesopores are able to be as "holders" to stabilize or anchor the gold nanoparticles to prevent further agglomeration or sintering. When tested in a probe reaction of CO oxidation, Au catalysts exhibit excellent activity and long-term stability with the complete CO conversion at 18 °C ($T_{50\%}$ = −11.2 °C) and reactive stability over 166 h under a space rate of 134,000 mL h^{-1} g_{cat}^{-1}. Potentially, such γ-Al_2O_3 nanorods with unique nanostructure can be a promising candidate for the preparation of high catalytic activity and stability catalysts.

Acknowledgement

The project was supported by National Program on Key Basic Research Project (973 Program, No.2013CB934104).

Appendix A. Supplementary data

Supplementary data (the activity result of Au/Al_2O_3 catalyst calcined at 700 °C and some recent result summary of alumina nanorods or nanofibers prepared by hydrothermal method) associated with this article can be found, in the online version, at http://dx.doi.org/10.1016/j.micromeso.2013.07.028.

References

[1] N.N. Nassar, A. Hassan, P.P. Almao, Energy Fuels 25 (2011) 3961–3965.
[2] Q. Yuan, H.H. Duan, L.L. Li, Z.X. Li, W.T. Duan, L.S. Zhang, W.G. Song, C.H. Yan, Adv. Mater. 22 (2010) 1475–1478.
[3] C.K. Costello, J.H. Yang, H.Y. Law, Y. Wang, J.N. Lin, L.D. Marks, M.C. Kung, H.H. Kung, Appl. Catal. A 243 (2003) 15–24.
[4] Y. Wei, R. Yang, Y.X. Zhang, L. Wang, J.H. Liu, X.J. Huang, Chem. Commun. 47 (2011) 11062–11064.
[5] W.Q. Cai, J.G. Yu, M. Jaroniec, J. Mater. Chem. 20 (2010) 4587–4594.
[6] G.F. Zhao, M. Ling, H.Y. Hu, M.M. Deng, Q.S. Xue, Y. Lu, Green Chem. 13 (2011) 3088–3092.
[7] A.F. An, A.H. Lu, Q. Sun, J. Wang, W.C. Li, Gold Bull. 44 (2011) 217–222.
[8] Y.F. Han, Z. Zhong, K. Ramesh, F. Chen, L. Chen, J. Phys. Chem. C 111 (2007) 3163–3170.
[9] Q. Yuan, A.X. Yin, C. Luo, L.D. Sun, Y.W. Zhang, W.T. Duan, H.C. Liu, C.H. Yan, J. Am. Chem. Soc. 130 (2008) 3465–3472.
[10] H.C. Lee, H.J. Kim, S.H. Chung, K.H. Lee, H.C. Lee, J.S. Lee, J. Am. Chem. Soc. 125 (2003) 2882–2883.
[11] T. Kim, J. Lian, J. Ma, X. Duan, W. Zheng, Cryst. Growth Des. 10 (2010) 2928–2933.
[12] H.S. Roh, G.K. Choi, J.S. An, C.M. Cho, D.H. Kim, I.J. Park, T.H. Noh, D.W. Kim, K.S. Hong, Dalton Trans. 40 (2011) 6901–6905.
[13] L. Zhang, X. Jiao, D. Chen, M. Jiao, Eur. J. Inorg. Chem. (2011) 5258–5264.
[14] H.Y. Zhu, J.D. Riches, J.C. Barry, Chem. Mater. 14 (2002) 2086–2093.
[15] Z. Zhu, H. Sun, H. Liu, D. Yang, J. Mater. Sci. 45 (2010) 46–50.
[16] W.Q. Cai, Y.Z. Hu, J. Chen, G.X. Zhang, T. Xia, CrystEngCommun 14 (2012) 972–977.
[17] M.G. Ma, Y.J. Zhu, Z.L. Xu, Mater. Lett. 61 (2007) 1812–1815.
[18] T.B. He, L. Xiang, S.L. Zhu, CrystEngCommun 11 (2009) 1338–1342.
[19] T.B. He, L. Xiang, S.L. Zhu, Langmuir 24 (2008) 8284–8289.
[20] S.C. Shen, Q. Chen, P.S. Chow, G.H. Tan, X.T. Zeng, Z. Wang, Reginald B.H. Tan, J. Phys. Chem. C 111 (2007) 700–707.
[21] M.G. Ma, Y.J. Zhu, G.F. Cheng, Y.H. Huang, J. Mater. Sci. Technol. 24 (2008) 637–640.
[22] P. Benito, M. Herrero, C. Barriga, F.M. Labajos, V. Rives, Inorg. Chem. 47 (2008) 5453–5463.
[23] Z.S. Wu, Y.D. Shen, Y. Dong, J.Q. Jiang, J. Alloys Compd. 467 (2009) 600–604.
[24] Y.L. Feng, W.C. Lu, L.M. Zhang, X.H. Bao, B.H. Yue, Y. Lv, X.F. Shang, Cryst. Growth Des. 8 (2008) 1426–1429.
[25] G. Stoica, J. Pérez-Ramírez, Chem. Mater. 19 (2007) 4783–4790.
[26] G.J. Ji, M.M. Li, G.H. Li, G.M. Gao, H.F. Zou, S.C. Gan, X.C. Xu, Powder Technol. 215–216 (2012) 54–58.
[27] R.L. Penn, J.F. Banfield, Science 281 (1998) 969–971.
[28] M.M. Schubert, S. Hackenberg, A.C. van Veen, M. Muhler, V. Plzak, R.J. Behm, J. Catal. 197 (2001) 113–122.
[29] W.F. Yan, Z. Ma, S.M. Mahurin, J. Jiao, E.W. Hagaman, S.H. Overbury, S. Dai, Catal. Lett. 121 (2008) 209–218.
[30] H.H. Kung, M.C. Kung, C.K. Costello, J. Catal. 216 (2003) 425–432.
[31] M. Okumura, S. Nakamura, S. Tsubota, T. Nakamura, M. Azuma, M. Haruta, Catal. Lett. 51 (1998) 53–58.
[32] J.T. Calla, M.T. Bore, A.K. Datye, R.J. Davis, J. Catal. 238 (2006) 458–467.
[33] G.H. Wang, W.C. Li, K.M. Jia, B. Spliethoff, F. Schüth, A.H. Lu, Appl. Catal. A 364 (2009) 42–47.